Application Development with Finite Element Method to Calculate Photogeneration Rate and Open-Circuit Voltage of Dye Sensitized Solar Cell

Zoltan Varga
Doctoral School of Applied Informatics and Applied Mathematics at the Óbuda University
Department of Natural Sciences at the Institute of Electrophysics, Kandó Kálmán Faculty of Electrical Engineering at the Óbuda University
Budapest, Hungary
varga.zoltan@uni-obuda.hu
ORCID 0000-0003-4692-1078

Ervin Racz
Department of Natural Sciences at the Institute of Electrophysics, Kandó Kálmán Faculty of Electrical Engineering at the Óbuda University
Budapest, Hungary
racz@uni-obuda.hu
ORCID 0000-0002-7692-1397

Abstract—**Amongst the several alternative resources, renewable energy source (RES) can provide continuous and clean energy. Furthermore, RESs have received a worldwide attention and an outstanding role is attributed to them. The sun energy can be exploited using light energy conversion applications such as photovoltaics. Dye Sensitized Solar Cell (DSSC) is third-generation photovoltaic device and a forward-looking, easily producible solar cell. Nevertheless, buying a commercially available DSSC, datasheet and material information are unavailable. Thus, the purchased DSSC is a black box. The main motivation is that to develop a MatLab application which is able to determine the material information and parameters of the Dye Sensitized Solar Cell from some incoming parameters. The goal of the study is to describe the operation of the developed MatLab application which calculated the photogeneration rate in function of the thickness of the cell, the open-circuit voltage, and to illustrate its operation via an example. The photogeneration rate is solved using the numerical finite element method as a numerical procedure. In our model the Beer-Lambert law is implemented. The model takes into consideration the measured parameters of the light such as photoncount-wavelength spectrum, transmission-wavelength spectrum and irradiation intensity-wavelength spectrum. Furthermore, the open-circuit voltage is an elementary electric parameter of a solar cell.**

Keywords—*Dye Sensitized Solar Cell, DSSC, Photogeneration Rate, Open-Circuit Voltage, Modelling, Numerical Solution*

I. INTRODUCTION

The current demand for electricity is exceptionally high. Furthermore, the growth of population and economy means an increasing need for the electricity [1]. The concentration of the carbon-dioxide (CO_2) in the atmosphere has been significantly rising, conforming that the present trends and previous centuries energy generation methods are doubtful [2]. Thus, researchers looking for solutions in order to decrease or normalize this great deal of CO_2 emission and to fulfill the energy need [3]. On the other hand, the EU's Energy Union strategy towards the carbon neutrality also influence the research area [4]. Amongst the several alternative resources, renewable energy sources can provide continuous and clean energy [5]. On the other hand, renewable energy sources have received a worldwide attention and an outstanding role is

attributed to them [6]. The sun energy can be exploited using light energy conversion applications such as photovoltaics, thermal collectors, and concentration solar power systems [7]. The photovoltaics directly converts the sunlight into electricity. One of the greatest advantages of the solar cell is that it does not emit carbon-dioxide and harmful gasses during its operation. Amongst the good deal of types of solar cells, the Dye Sensitized Solar Cell (DSSC) is a third generation, forward looking, easily producible solar cell which made a remarkable progress [8]. The conventional commercialized modules dominant the markets, however, DSSC has received a broad recognition [9]. Although, Dye Sensitized Solar Cell must face with a great deal of challenges in order to take a wider part in the global PV market [10]. The potential opportunities of DSSC paved a way for research interest [11]. From the extensive amount of experimental work to optimize the DSSC made it clear that the mathematical modelling of DSSC is highly recommended.

The first breakthrough Dye Sensitized Solar Cell was fabricated by Brian O'Regan and Michael Greatzel in 1991 [12]. The reported overall incident photon to current conversion efficiency yield was $7.1 – 7$-9% in simulated light, and this reported number was exceeded in 1993 with 9.6%, and then in 1997 with 10% [10]. However, the conversion efficiency has been progressing, the gains are relatively slow. The achieved word record of the conversion efficiency was 14% by M. Greatzel presented at the Hybrid and Organic Photovoltaic conference [13]. The conventional Dye Sensitized Solar Cell contains of five main components: (i) a glass substrate with transparent conductive oxide (TCO); (ii) n-type semiconductor layer with a wide bandgap, which is most commonly titanium-dioxide (TiO_2); (iii) dye sensitizer absorbed on the surface of the TiO_2; (iv) electrolyte containing iodide-triiodide (I^-/I_3^-) couples; and (v) counter electrode, commonly formed from platinum (Pt) [14]. The TiO_2 working electrode layer absorb only a small fraction of the UV region of the light. On the other hand, other semiconductor materials are also used for the deposition of the thin layer such as ZnO, SnO_2 [15]. Furthermore, there are requirements for the dye sensitizer as well. It has to be able to cover a wide spectral range, from the ultraviolet to the near-infrared regions. Standard dyes such as N3, N719 and N749 are commercially

available; however, research also deals with natural dyes such as extracts of fruits (raspberry, blueberry) and leaves [16], [17]. Moreover, it is highlighted that the energy level of the excited state for the dye (shown as E_{CB} in Fig. 1.). Without the higher state of the dye, it is impossible to enable electron injection to the n-type semiconductor layer [18]. The used electrolyte, such as I^-/I_3^-, has five main components which are the additives, solvent, ionic liquids, redox couple, and cations. Because of the oxidization of the dye, redox couple should be able to regenerate the oxidized dye. On the other hand, electrolyte should have long-term thermal and chemical stability. Counter electrode, such as Pt, collects holes from the hole transport materials. Taking into account, that platinum has a high cost, several alternatives have been developed in order to replace it in Dye Sensitized Solar Cell. These substitutes are the carbon, carbonyl sulfide [11].

Fig. 1 illustrates the energy diagram of the DSSC with the direction of electron flow. When DSSC is exposed to sunlight, the dye molecules get excited and oxidized upon absorption of sunlight and in turn they inject electrons into the conduction band of the n-type TiO_2 semiconductor, the electron diffuses to the electrode, front contact, then exists to the external load. The oxidized dye molecules are regenerated by the electrolyte which collect the electrons from the counter electrode. Ideally, the open-circuit voltage (V_{OC}) is determined by the potential difference between the Fermi level of the electrons in the semiconductor film and the redox potential of the electrolyte [8]. The performance of a DSSC is on the bases of the low recombination rate, the remarkable visible light harvesting, relatively fast electron transport and the charge separation [19].

Bose et al. compared the performance of the DSSC module with the Silicon (Si)-based module. According to their results, the performance of the DSSC module in function of temperature is better than the Si-based one [20]. On the other hand, there is a significant difference between the working principle of the DSSC and the Si-based solar cell. While in case of the Si-based solar cell the semiconductor layer absorbs and divides the charge carrier, in case of the DSSC, the absorption and electron transfer are done separately [21].
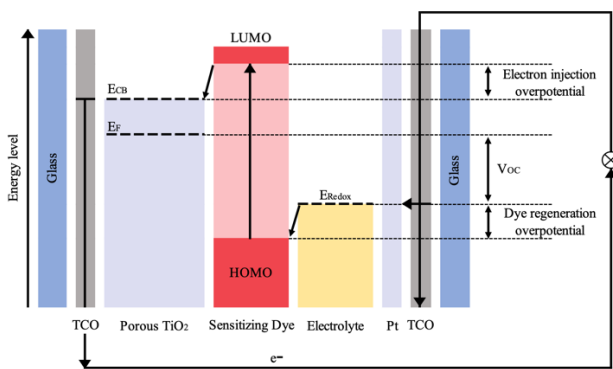

Fig. 1. Energy diagram of the Dye Sensitized Solar Cell with the direction of electron flow, where the light blue reresent the glass, the grey parts are the transparent conductive oxide (TCO), the light purpule is the porous titanizm dioxide (TiO_2) and the platinum (Pt), the reddish part represents the sensitizing dye in the Highest Occupied Molecular Orbital (HOMO) and the Lowest Unoccupied Molecular Orbital (LUMO), and the light yellow means the electrolyte [19].

There is an extensive amount of experimental work to optimize the performance of the Dye Sensitized Solar Cell.

However, the material research is undisputedly important, the mathematical modelling of the Dye Sensitized Solar Cell is highly recommended. The first simulation of the DSSC model was introduced in 1994, associated with Sven Södergren. The photoelectrochemical behavior of the DSSC was theoretically investigated [22]. After a short time, in 1998, Ferber established a macroscopic-scale model and it has been widely adopted to understand electron transport in TiO_2 [23]. The work of Le Bahers et al. reflected that it is crucial to setup a computational protocol which is able to study the properties of the dye-semiconductor interface and not only the properties of the isolated dye [24]. Listorti et al. reviewed the electron transfer dynamics in Dye Sensitized Solar Cell [25]. Usuma et al. theoretically examined the application of light scattering of submicron titanium-dioxide particles to dye-sensitized nanocrystalline photochemical cells. In the work, Monte Carlo simulation was applied, and the results revealed that the increase of absorption path length of photons in the TiO_2 layer improves the light absorption [26]. Nelson et al. experimentally investigated the photoconductivity of symmetrically contacted TiO_2 layer based on different chemical environments. Furthermore, a physical model which is capable of explain the results of the experiment is introduced [27]. Gecami et al. reported numerical solutions for electron transport in the carbon nano-tube (CNT) electrode. In order to simulate the electron transport, photogeneration rate was calculated [28]. Rothenberger et al. presented a model which is able to estimate the enhancement of optical absorption. The absorption is obtained from the light scattering and from the reflection. Nevertheless, the light scattering occurs in the porous nanocrystalline films and the reflection occurs at the back electrode [29]. Onodera et al. modelled the DSSC on the basis of the titanium-dioxide electrode structure model. In the model macro-scale numerical simulation was used to analyte the electric current–electric voltage characteristics of the Dye-Sensitized Solar Cell [30]. Muhammad Habieb et al. analyzed the electric current–voltage curve of the DSSC using numerical calculations. In the work, neither the photogeneration rate nor the MatLab program were not discussed in great details [31]. Korfiatas et al. numerically modelled a titanium-dioxide DSSC based on the continuity and transport equations for all charge species involved in the system. Mitroi et al. proposed a numerical procedure and a numerical method to optimize the performance of DSSCs. The proposed numerical procedure consisting of a simplified model, is applied on a classical DSSC. In the work, the real rate of absorbed photons is calculated via introducing a factor. The value of the factor is between 0 and 1 constant. This factor simplifies the light absorption and reflection on transport conductive oxide (TCO) electrode [32]. According to the studied literature, the photogeneration rate in function of the thickness of the cell was integrated in the wavelength range between 300 nm and 800 nm. The range above 800 nm is the heat radiation which heats the surface of the cell resulting reduction of the electrical properties of the cell. In other words, the accumulated heat reduces the maximum power point and the efficiency of the cell. On the other hand, it is also seen that numerical simulation was commonly used in the literature.

Nevertheless, buying a commercially available Dye Sensitized Solar Cell, datasheet and material information are unavailable. Thus, the purchased DSSC is a black box without any information. Furthermore, designing and building a state-of-the-art DSSC is a costly process because of the

investigation machines. The main motivation is to develop such a MatLab application that is able to determine the material parameters from the light parameters such as incoming photoncount–wavelength spectrum, incoming irradiation intensity–wavelength spectrum, transmittance–wavelength spectrum and from the electric current–voltage characteristics. The goal of the study is describing the operation of the developed MatLab application which calculates the photogeneration rate in function of the thickness of the cell and the open-circuit voltage and illustrating its operation via an example. The photogeneration rate is solved using the numerical finite element method as a numerical procedure. In our model the Beer-Lambert law is implemented. The model takes into consideration the measured parameters of the light. Furthermore, the open-circuit voltage is calculated from the photogeneration rate which is an elementary electric parameter of a solar cell. On the other hand, from the above-mentioned literature, it is seen that, application for the mentioned problem has not been developed. The preliminary code was presented in [19], thus this paper is an extension of that paper.

## II. THEORY OF THE PHOTOGENERATION

Photogeneration is an important part of the working principle for DSSC. In the photogeneration process the absorbed photons generate an excited state. So, the dye molecular are excited (S^*) from the ground state (S) where $h\nu$ is the energy of the photon [11]:

$$S + h\nu \rightarrow S^* \qquad (1)$$

Due to the exciton the electron (e^-) diffuses through to the semiconductor (TiO_2) to the TCO to enter the external load:

$$S^* \rightarrow S^+ + e^- \qquad (2)$$

The oxidized dye molecules (S^+) are regenerated by the reducing species of the redox couple (I^-/I_3^-):

$$3I^- \rightarrow I_3^- + 2e^- \qquad (3)$$

$$S^+ + e^- \rightarrow S \qquad (4)$$
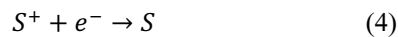
The oxidized mediator (I_3^-) reduces to ($3I^-$) via diffusing towards the counter electrode:

$$I_3^- + 2e^- \rightarrow 3I^- \qquad (5)$$

The sensitized dye must meet electronic and optical requirements such as (1) the Lowest Unoccupied Molecular Orbital (LUMO) must align up to the edge of the conduction band of the titanium-dioxide; (2) the Highest Occupied Orbital (HOMO) must be lower than the redox potential of the electrolyte; and (3) it should have a wide absorption wavelength spectrum [18]. The excitation depends on the absorption – wavelength spectrum of the sensitized dye. The absorbed dye shows great activity in the range of 300 nm to 800 nm. The dye-semiconductor-electrolyte structure can be regarded as a homogeneous medium with a uniform absorption-wavelength spectrum or absorption coefficient ($\alpha(\lambda)$) because the semiconductor and electrolyte have negligible $\alpha(\lambda)$ [19]. The Beer-Lambert law describes the rate of light absorption through the material. The law states that there is proportionality between the amount of absorption and

the concentration of the absorber, and an equal fraction of the incoming light are absorbed by the successive layer of the sensitized dye [33].

Furthermore, there is a connection between the absorption-wavelength function and the photogeneration rate which can be expressed by the following equation:

$$G_e(x) = \int_{\lambda_1}^{\lambda_2} \phi(\lambda)\alpha(\lambda)e^{-\alpha(\lambda)x}\, d\lambda \qquad (6)$$

where $\phi(\lambda)$ is the photon count–wavelength spectrum, $\alpha(\lambda)$ is the absorption–wavelength spectrum and $x\epsilon[0,d]$ and it described the position inside the TiO$_2$ film, including the dye, with a thickness of d.

According to Gong et al. the absorption coefficient $\alpha(\lambda)$ at wavelength (λ) can be expressed as [18]:

$$\alpha(\lambda) = \frac{A_{abs}(\lambda)}{d} \qquad (7)$$

where $A_{abs}(\lambda)$ is expressed as:

$$A_{abs}(\lambda) = -\ln\left[\frac{T(\lambda)}{I(\lambda)-R(\lambda)}\right] \qquad (8)$$

where $T(\lambda)$ is the transmission intensity–wavelength spectrum, $I(\lambda)$ is the irradiation intensity–wavelength spectrum and $R(\lambda)$ is the reflection intensity–wavelength spectrum. Fig. 2. shows the schematic of the simplified model in one dimension with the light parameters.
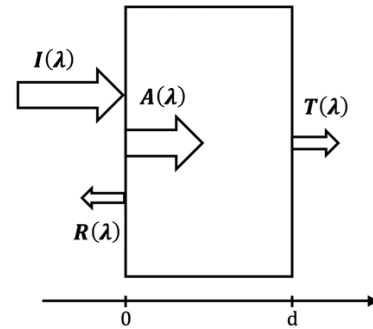

Fig. 2. Schematic of the simplified cell in one dimension where $I(\lambda)$ is the irradiation intensity–wavelength spectrum, the $T(\lambda)$ is the transmission–wavelength spectrum, the $A(\lambda)$ is the absorbance–wavelength spectrum and $R(\lambda)$ is the reflection–wavelength spectrum. $I(\lambda) = A(\lambda) + T(\lambda) + R(\lambda)$

Table I. shows the absorption spectra and electrical open-circuit voltage of DSSC on the basis of different dye sensitizers. The N3, N719, N749, and Z907 dye sensitizers are commonly used in DSSCs. The dragon fruit, red rose, lawsonia inermus leaves are extracts from fruits and leaves.

According to Gokilamani et al. the maximum absorption coefficient of the red rose is fifteen times higher than the maximum absorption coefficient of the N719 dye [34].

Dye	Absorption maxima (nm)	V_{OC} (V)	Reference
N3	518 and 380 534	0.72	[10], [35]
N719	532	0.846	[36]
N749	605	0.72	[37]
Z907	526	0.722	[38]
Dragon fruit	535	0.22	[39]
Red rose	535	0.48	[34]
Lawsonia inermus leaves	518	0.61	[40]

The equation (6) was converted into equation (9) and the following is got:

$$G_e(x) = \sum_{i=1}^{n} \sum_{j=1}^{m} \left(\phi(\lambda_i) \cdot \alpha(\lambda_i) \cdot e^{-\alpha(\lambda_i) \cdot x_j} \right) \quad (9)$$

The $I(\lambda)$, $T(\lambda)$ parameters are measured using Apogee PS-100 spectroradiometer which wavelength sensitivity is between 350 nm and 1150 nm. According to the studied measuring devices, the upper wavelength sensitivity does not exceed the 1150 nm upper limit. On the other hand, solar cell does not absorb more than 20% of the irradiance in the infrared region. Therefore, the application solves the photogeneration rate in function of the thickness of the cell in the wavelength region between 350 nm and 800 nm. Fig. 3. shows the AM 1.5G spectrum normalized to $1000 \ W/m^2$. The spectrum is divided into three parts: visible light, IR radiation, electric power. From the figure it is seen that the solar cell does not use the majority of the incoming spectrum. Moreover, the infrared region is the heat region which mostly heat the surface of the solar cell which has a reduction effect on the electric parameters.
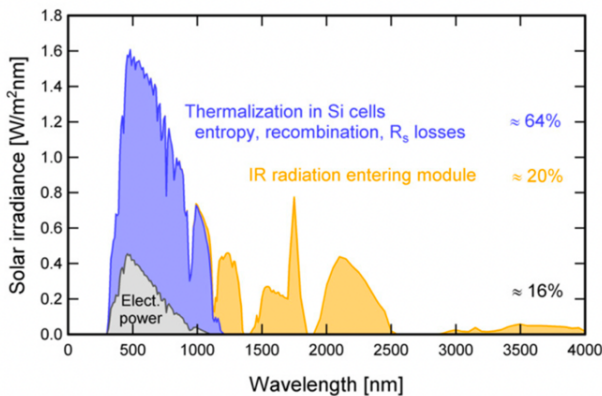

Fig. 3. AM 1.5G spectrum normalised to 1000 W/m² [41]. The spectrum is devided into three part: visible light represented with blue, electric power generator part seen with grey color, and the yellow part which represents the infrared zone of the spectrum.

Simplified model is taken into consideration when the electrical transport is purely diffusive. On the other hand, other simplifications are also used such as the internal electric field generated by unbalanced local charge is neglected. Therefore, the electron density in the conduction band of the n-type semiconductor layer is described with the following continuity equation:

$$-\frac{1}{e} \frac{dJ(x)}{dx} = G_e(x) - R(x) \quad (10)$$

where $R(x)$ is the recombination rate, and the J is the electric current density and can be expressed as:

$$J(x) = eD \frac{dn(x)}{dx} \quad (11)$$

where $n(x)$ is the electron density in the position inside the titanium-dioxide, e is the elementary charge, D is the electron diffusion coefficient, and x is the one-dimension position inside the semiconductor. Furthermore, the trapping and detrapping processes are also neglected [42]. Additionally, it is assumed that the recombination process takes places between the electrons from the conduction band of the n-type semiconductor layer and the anions in the electrolyte solution, and it is given with the following equation [43]:

$$R(x) = \frac{n(x) - n(0)}{\tau} \quad (12)$$

where τ is the electron lifetime, and $n(0)$ is the electron density in the dark. Mitroi et al. used the following two boundary conditions which are the following [32]:

1) *The boundary condition at $x = 0$ is*

$$n(x)|_{x=0} = N_c e^{-\frac{E - eV}{k_B T}} \quad (13)$$

where N_c is the density of the states in the conduction band of n-type semiconductor layer, and it is given by:

$$N_c = 2 \left(\frac{2 \pi m_e^* k_B T}{h^2} \right)^{\frac{3}{2}} \quad (14)$$

where E is the energy between the conduction band edge and the Fermi quasi level, V is the voltage, k_B is the Boltzmann constant, T temperature, m_e^* is the effective mass of electron, and h is the Planck constant.

2) *The boundary condition at $x = d$*

$$\frac{dn(x)}{dx} \bigg|_{x=d} = 0 \quad (15)$$

As a result of the process the open-circuit voltage (V_{OC}) is given by the following equation:

$$V_{OC} = \frac{k_B T \ln \left[\frac{\tau G_e(0) + n_0}{N_c} \right] + E}{e} \quad [32] \ (16)$$

where $G_e(0)$ is photogeneration at $x = 0$. The V_{OC} is derived the condition when the electric current density is zero ($J = 0$).

III. DEVELOPED APPLICATION

In this chapter the developed MatLab application is described in great details. The aim of the developed application is to calculate the photogeneration rate in function of the thickness of the cell and the open-circuit voltage as an elementary electric parameter of the DSSC. In order to calculate the photogeneration in function of the cell thickness numerical finite element method is used which is a numerical technique. The finite element method (FEM) produces sets of discrete numerical approximations. Fig. 4. shows the flow chart of the developed application with the input parameters and with the output parameters. The flow chart shows the separate steps of the process in sequential order.
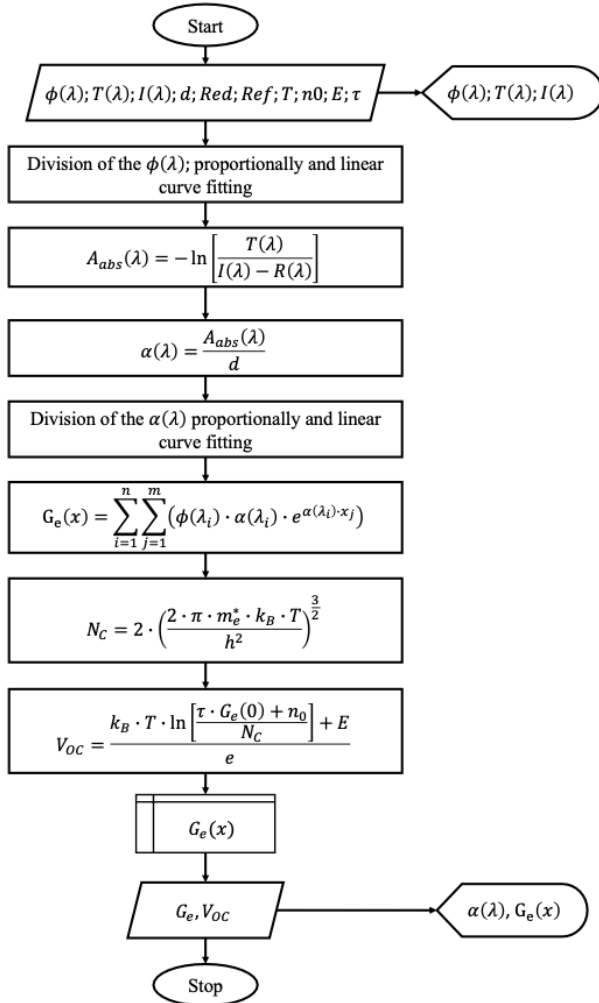

Fig. 4. The flow chart of the developed MatLab application where Red means the reduction, Ref represents the reflection. The steps of the processes are in sequential order.

1) The input parameters: From the imput parameters the thickness of the cell (d) in μs, the reduction (Red) in %, the reflection (Ref) in %, the temperature (T) in K, the electron density in the dark (n_0) in cm^{-3}, the energy between the conduction band and the Fermi level (E) in eV, and the electron lifetime (τ) in ms are numerical fields. Furthermore, the photoncount–wavelength spectrum ($\phi(\lambda)$), the transmission–wavelength spectrum ($T(\lambda)$), and the irradiation intensity–wavelength soectrum ($I(\lambda)$) can be imported from a txt file. These functions are available using

buttons. Howver, the reflection of the surface is difficult to determine quantitatively, a numerical field is available. According to Gong et al. it is advasiable to take as 4% [18]. On the other hand, minor calculations are also done since the photoncount–wavelength spectrum has to be per surface unit. After importing the incoming parameters, these parameters are plotted. The important parameters are stored and write into table in the application.

2) Photoncount–wavelength division: The photoncount–wavelength spectrum is divided the interval of [350 nm, 800 nm] into 90 equal subintervals of length of 10. Moreover, the subintervals are not overlap each other, so the subintervals are disjucts sets. Fig. 5. shows the numerical procedure for dividing interval of [a,b] into n equal intervals of leght of h, where n is equal to 90, and h is equal to 10. However, the this devision is computer consuming process, the results can be considered as an appropriate approach.
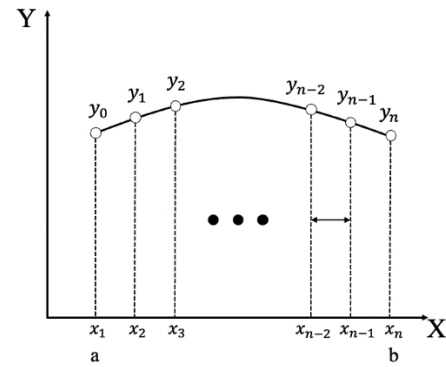

Fig. 5. Numerical procedure for dividing interval of [a,b] into n equal subintervals of length h.

After the division, in each subintervals linear curve is fitted, expressed by the following:

$$y = a \cdot x + b \tag{17}$$

where a and b are coefficients of the linear function. These parameters are used in the calculation of the photogeneration rate.

3) Solving absoprtion–wavelength spectrum: As a next step of the application is to solve the absoprtion–wavelength spectrum based on equation (7) and equation (8). The absoprtion in function of the wavelength is not plotted immediately, however, the application saves the data and it is plotted after the calculation of the open-circuit voltage. The solved absoprtion–wavelength data is stored in table in the application.

4) Absoprtion–wavelength division: As in the photoncount–wavelength spectrum division, absortion–wavelength spectrum is divided with the same numerical method. The absoprtion–wavelength spectrum is divided the interval of [350 nm, 800 nm] into 90 equal subintervals of length of 10. Furthermore, in each subintervals linear curve is fitted and the fitted coefficients are determined.

5) Numerical calculation of the photogeneration rate: After the division of the photoncount-wavelength spectrum and the division of the absoprtion-wavelength spectrum, the

photogeneration rate in function of the thickness of the cell was calculated numerically by the equation (9). The step size is set to 1 nm which is also time consuming process, but the result is detailed.

6) Open-circuit voltage calculation: Using the first number of the photogeneration table, the open-circuit voltage is calculated by the equation (14) and equation (16). Depending on the parameters written in the numerical field, the calculation is done. After the calculation, the photogeneration rate in function of the thickness of the cell, and the absoprtion-wavelength spectrum is plotted. On the other hand, these values are written into table and stored by the application. The two most important parameters such as photogeneration (G_e) and open-circuit voltage (V_{OC}) are written into main page. The photogeneration rate in fuction of the cell thickness can be exported and saved to .txt file.

IV. EXAMPLE OF THE OPERATION OF THE APPLICATION

In this chapter, an example of the operation of the developed MatLab application is shown. Fig. 6. shows the designed and built MatLab application. From the figure it can be concluded that on the left side the data selection is seen. Thus, the numerical fields, the data importing buttons are located on the left side. Nevertheless, the figures and tables are on the right side.
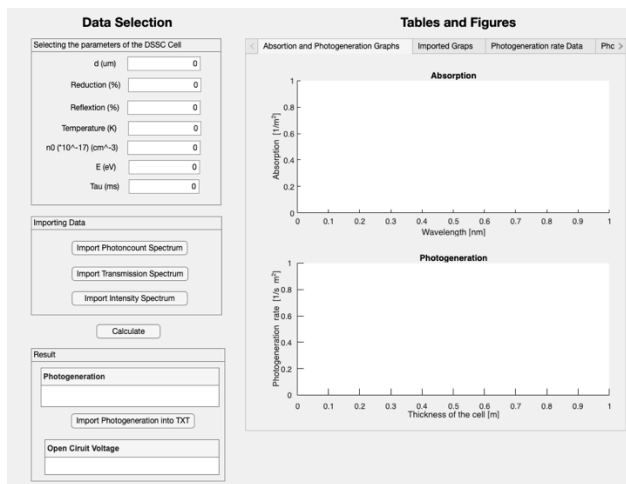

Fig. 6. Designed and built MatLab application opening page. The taken picture is a screenshot about the application. The application surface is more visible on the real screen. Thus, the visibility in the monitor is appropriate. On the left side in the numeric filds the following can be seen from the top: thickness of the cell $(d\ (um))$, Reduction (%), Reflection (%), Temperature (K), electron density in the dark $(n0\ (*10^\wedge-17)\ (cm^\wedge-3))$, energy difference between the conduction band and the Fermi level $(E\ (eV))$, electron lifetime $(Tau\ (ms))$. On the left side in the middle section the import of the .txt file buttons such as the "Import Photoncount Spectrum", "Import Transmission Spectrum", "Import Intensity Spectrum" are seen. Under these buttons the "Calculate" button is located. Clicking on these button, the photogeneration rate in function of the thickness of the cell $(G_e(x))$, and the open-circuit voltage (V_{OC}) are calculated. If the calculations are done the G_e and V_{OC} are written in the tables under the "Calculate" button. On the right side the tables and the figure can be seen.

Figure 7. shows the example of the operation of the MatLab application. On the lift side, the input parameters are seen. Table II. shows the input parameters to clarify the operation example shown in Fig. 7.
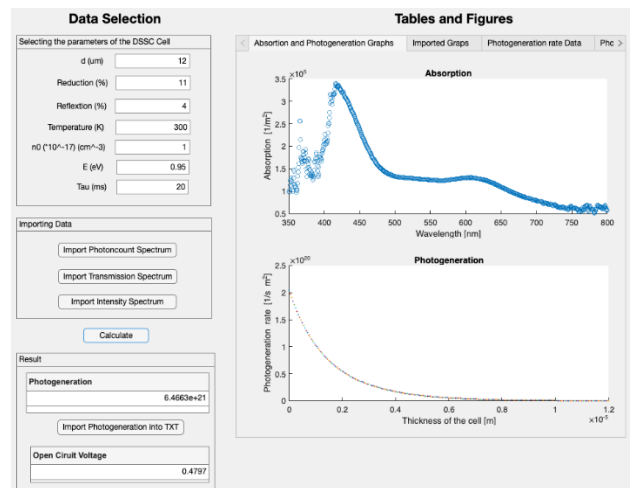

Fig. 7. Example of the operation of the MatLab application. Table II. contains the written parameters to make clarify the operation example. The dimension of the calculated photogeneration rate is in 1/(s m²) and the dimension of the calculated open-circuit voltage is in V.

In Fig. 7. the absorption–wavelength scatter plot in seen and under that the photogeneration rate in function of the thickness of the cell is shown. Furthermore, the calculated photogeneration rate is $6.4663 \cdot 10^{-21}\ \frac{1}{s\,m^2}$ and the calculated open-circuit voltage is $0.4797\ V$.

TABLE II. INPUT PARAMETERS FOR THE OPERATION EXAMPLE

Parameter	Symbol	Value	Dimension
Thickness of the cell	d (um)	12	μm
Reduction	Reduction (%)	11	%
Reflection	Reflection (%)	4	%
Temperature	Temperature (K)	300	K
Electron density in the dark	n0 (*10^-17) (cm^-3)	1	cm^{-3}
Electron lifetime	Tau (ms)	20	ms

Comparing the calculated open-circuit voltage with the content of Table I., it can be concluded that the calculated V_{OC} is a possible value.

V. SUMMARY AND CONLSUION

The main motivation is to develop a MatLab application which is capable of determining the material information and parameters of the DSSC from the incoming parameters because purchasing a commercially available DSSC does not contain datasheet and other material information, thus, these cells are considered as black boxes. The goal of the study is to describe the operation of the developed MatLab application which calculates the photogeneration rate in function of the thickness of the cell, calculates the open-circuit voltage and to illustrate its operation via an example. Taking the photoncount–wavelength spectrum, transmission–wavelength spectrum, the irradiation intensity–wavelength spectrum and

the thickness of the cell into consideration, the photogeneration rate is solved in function of the cell thickness. On the other hand, in order to calculate the photogeneration in function of the cell thickness numerical finite element method is used which is a numerical technique The open-circuit voltage is solved using the photogeneration rate in $x = 0$ point. The example represents the operation of the MatLab application clearly. Moreover, the application can be regarded as user friendly with the numeric fields and with the buttons. The desired parameters will be shown in the main page after the calculation. Also, the photogeneration rate can be exported into .txt file.

The difference in the working principle between Mitroi et al. and the current one is that in this study the open-circuit voltage is calculated from the photogeneration rate obtained from the calculations from experimental data. The application is Apogee PS-100 device-dependent because the calculations are remarkably done if the data comes from the mentioned device. On the other hand, authors also plan to use data smoothing technique to smooth the absorption–wavelength spectrum, thus reducing the probabilities of inaccuracies and error resulting from the experiment. Nevertheless, it is also included in the outlook that authors will continue the work in order to fulfill the main motivation in the future. Moreover, from the studied literature, it is seen that application for the mentioned problem has not been developed.

The authors declare no conflict of interest.

REFERENCES

[1] S. J. Davis and K. Caldeira, 'Consumption-based accounting of CO₂ emissions', *Proceedings of the National Academy of Sciences*, vol. 107, no. 12, pp. 5687–5692, Mar. 2010.

[2] M.-E. Ragoussi and T. Torres, 'New generation solar cells: concepts, trends and perspectives', *Chem. Commun.*, vol. 51, no. 19, pp. 3957–3972, 2015.

[3] S. Perry, J. Klemes, and I. Bulatov, 'Integrating waste and renewable energy to reduce the carbon footprint of locally integrated energy sectors', *Energy*, vol. 33, no. 10, pp. 1489–1497, Oct. 2008.

[4] J. J. Fierro, A. Escudero-Atehortua, C. Nieto-Londono, M. Giraldo, H. Jouhara, and L. C. Wrobel, 'Evaluation of waste heat recovery technologies for the cement industry', *International Journal of Thermofluids*, vol. 7–8, p. 100040, Nov. 2020.

[5] A. K. Pandey, V. V. Tyagi, J. A. Selvaraj, N. A. Rahim, and Sk. K. Tyagi, 'Recent advances in solar photovoltaic systems for emerging trends and advanced applications', *Renewable and Sustainable Energy Reviews*, vol. 53, pp. 859–884, Jan. 2016.

[6] S. Malakar, S. Goswami, B. Ganguli, A. Chakrabarti, S. S. Roy, K. Boopathi, A. G. Rangaraj, Deep-Learning-Based Adaptive Model for Solar Forecasting Using Clustering', *Energies*, vol. 15, no. 10, p. 3568, May 2022.

[7] M. Malinowski, J. I. Leon, and H. Abu-Rub, 'Solar-Photovoltaic and Thermal Energy Systems: Current Technology and Future Trends', *in Proceedings of the IEEE*, vol. 105, no. 11, pp. 2132–2146, Nov. 2017.

[8] J. Gong, K. Sumathy, Q. Qiao, and Z. Zhou, 'Review on dye-sensitized solar cells (DSSCs): Advanced techniques and research trends', *Renewable and Sustainable Energy Reviews*, vol. 68, pp. 234–246, Feb. 2017.

[9] V. Devabhaktuni, M. Alam, S. Shekara Sreenadh Reddy Depuru, R. C. Green, D. Nims, and C. Near, 'Solar energy: Trends and enabling technologies', *Renewable and Sustainable Energy Reviews*, vol. 19, pp. 555–564, 2013.

[10] K. Sharma, V. Sharma, and S. S. Sharma, 'Dye-Sensitized Solar Cells: Fundamentals and Current Status', *Nanoscale Res Lett*, vol. 13, no. 1, p. 381, Dec. 2018.

[11] S. Sharma, Bulkesh Siwach, S. K. Ghoshal, and D. Mohan, 'Dye sensitized solar cells: From genesis to recent drifts', *Renewable and Sustainable Energy Reviews*, vol. 70, pp. 529–537, Apr. 2017.

[12] B. O'Regan and M. Greatzel, 'A low-cost, high-efficiency solar cell based on dye-sensitized colloidal TiO₂ films', *Nature*, vol. 353, no. 6346, pp. 737–740, 1991.

[13] N. Tomar, A. Agrawal, V. S. Dhaka, and P. K. Surolia, 'Ruthenium complexes based dye sensitized solar cells: Fundamentals and research trends', *Solar Energy*, vol. 207, pp. 59–76, Sep. 2020.

[14] M. Kokkonen, P. Talebi, J. Zhou, S. Asgari, S. A. Soomro, F. Elsehrawy, J. Halme, S. Ahmad, A. Hagfeldt, S. G. Hashmi, 'Advanced research trends in dye-sensitized solar cells', *Journal of Materials Chemistry A*, vol. 9, no. 17, pp. 10527–10545, 2021

[15] M. Greatzel, 'Photoelectrochamical cells', *Nature*, vol. 414, pp. 338–344, 2001.

[16] S. Hao, J. Wu, Y. Huang, and J. Lin, 'Natural dyes as photosensitizers for dye-sensitized solar cell', *Solar Energy*, vol. 80, no. 2, pp. 209–214, Feb. 2006.

[17] M. Hosseinnezhad, K. Gharanjig, M. K. Yazdi, P. Zarrintaj, S. Moradian, M. R. Saeb, F. J. Stadler, 'Dye-sensitized solar cells based on natural photosensitizers: A green view from Iran', *Journal of Alloys and Compounds*, vol. 828, p. 154329, Jul. 2020.

[18] J. Gong and S. Krishnan, 'Mathematical modeling of dye-sensitized solar cells', *in Dye-Sensitized Solar Cells, Elsevier*, pp. 51–81, 2019.

[19] Z. Varga and E. Racz, 'A numerical model and a code development for photogeneration rate calculation for a dye sensitized solar cell' *in 2022 IEEE 16th International Symposium on Applied Computational Intelligence and Informatics (SACI)*, Timisoara, Romania, May 2022, pp. 000341–000346.

[20] S. Bose, V. Soni, and K. R. Genwa, 'Recent advances and future prospects for dye sensitized solar cells: A review', *International Journal of Scientific and Research Publications*, vol. 5, no. 4, p. 9, Apr. 2015.

[21] F. Schoden, M. Dotter, D. Knefelkamp, T. Blachowicz, and E. Schwenzfeier Hellkamp, 'Review of state of the art recycling methods in the context of dye sensitized solar cells' *Energies*, vol. 14, no. 13, p. 3741, Jun. 2021.

[22] S. Soedergren, A. Hagfeldt, J. Olsson, and S.-E. Lindquist, 'Theoretical models for the action spectrum and the current-voltage characteristics of microporous semiconductor films in photoelectrochemical cells', *J. Phys. Chem.*, vol. 98, no. 21, pp. 5552–5556, May 1994.

[23] J. Ferber, 'An electrical model of the dye-sensitized solar cells', *Solar Energy Materials and Solar Cells*, vol. 53, no. 1–2, pp. 29–54, May 1998.

[24] T. Le Bahers, T. Pauporté, P. P. Lainé, F. Labat, C. Adamo, and I. Ciofini, 'Modeling dye-sensitized solar cells: From theory to experiment', *J. Phys. Chem. Lett.*, vol. 4, no. 6, pp. 1044–1050, Mar. 2013.

[25] A. Listorti, B. O'Regan, and J. R. Durrant, 'Electron transfer dynamics in dye-seensitized solar cells', *Chem. Mater.*, vol. 23, no. 15, pp. 3381–3399, Aug. 2011.

[26] A. Usami, 'Theoretical simulations of optical confinement in dye-sensitized nanocrystalline solar cells', *Solar Energy Materials*, p. 11, 2000.

[27] J. Nelson, A. M. Eppler, and I. M. Ballard, 'Photoconductivity and charge trapping in porous nanocrystalline titanium dioxide', *Journal of Photochemistry and Photobiology A: Chemistry*, vol. 148, np. 1–3, pp. 25–31, May 2002.

[28] Y. Gacemi, A. Chekname, and H. S. Hilal, 'Simulation and modelling of charge transport in dye-sensitized solar cells based on carbon nano-tube electrodes', *Phys. Scr.*, vol. 87, no. 3, p. 035703, Mar. 2013.

[29] G. Rothenberger, P. Comte, and M. Gra, 'A contribution to the optical design of dye-sensitized nanocrystalline solar cells', *Solar Energy Materials*, p. 16, 1999.

[30] M. Onodera, K. Ogiya, A. Suzuki, H. Tsuboi, N. Hatakeyama, A. Endou, H. Takaba, M. Kubo, A. Miyamoto, 'Modeling of dye-sensitized solar cells based on TiO₂ electrode structure model' *Japanese Journal of Applied Physics.*, vol. 49, no. 4, p. 04DP10, Apr. 2010.

[31] A. Muhammad Habieb, M. Irwanto, I. Alkian, F. Khalimatus Sya'diyah, H. Widiyandari, and V. Gunawan, 'Dye-sensitized solar cell simulation performance using MATLAB', *Journal of Physics: Conference Series*, vol. 1025, no. 1, p. 012001, May 2018.

[32] M. R. Mitroi, L. Fara, and M. L. Ciurea, 'Numerical procedure for optimizing dye-sensitized solar cells', *Journal of Nanomaterials*, vol. 2014, pp. 1–6, 2014.

[33] B. Maldon and N. Thamwattana, 'Review of diffusion models for charge-carrier densities in dye-sensitized solar cells', *Journal of Physics Communications,* vol. 4, no. 8, p. 082001, pp. 1–18, Aug. 2020.

[34] N. Gokilamani, N. Muthukumarasamy, M. Thambidurai, A. Ranjitha, D. Velauthapillai, T. S. Senthil, R. Balasundaraprabhu, 'Dye-sensitized solar cells with natural dyes extracted from rose petals', *Journal of Materials Science: Materials in Electronics*, vol. 24, no. 9, pp. 3394–3402, Sep. 2013.

[35] D. Wei, 'Dye sensitized solar cells', *International Journal of Molecular Sciences*, vol. 11, no. 3, pp. 1103–1113, Mar. 2010.

[36] T. Funaki, M. Yanagida, N. Onozawa-Komatsuzaki, K. Kasuga, Y. Kawanishi, and H. Sugihara, 'A 2-quinolinecarboxylate-sunstituted ruthenium(II) complex as a new type of sensitizer for dye-sensitized solar cells', *Inorganica Chimina Acta*, vol. 362, no. 7, pp. 2519–25522, May 2009.

[37] A. S. Polo, M. K. Itokazu, and N. Y. Murakami Iha, 'Metal complex sensitizers in dye-sensitized solar cells', *Coordination Chemistry Reviews*, vol. 248, no. 13–14, pp. 1343–1361, Jul. 2004.

[38] N. Onozawa-Komatsuzaki, M. Yanagida, T. Funaki, K. Kasuga, K. Sayama, and H. Sugihara, 'Near-IR dye-sensitized solar cells using a new type of ruthenium complexes having 2,6-bis(quinolin-2-yl)pyridine derivatives', *Solar Energy Materials and Solar Cells*, vol. 95, no. 1, pp. 310–314, Jan. 2011.

[39] R. A. M. Ali and N. Nayan, 'Fabrication and analysis of dye-sensitized solar cell using natural dye extracted from dragon fruit', *International Journal of Integrated Engineering*, vol. 2, no. 3, p. 8, Dec. 2010.

[40] K. A. Aduloju, M. B. Shitta, and S. Justus, 'Effect of extracting solvents on the stability and performances of dye-sensitized solar cell prepared using extract from lawsonia inermis', *Fundamental J. Modern Physics*, vol. 1, no. 2, pp. 261–268, Oct. 2011.

[41] M. R. Vogt, H. Holst, M. Winter, R. Brendel, and P. P. Altermatt, 'Numerical Modeling of c-Si PV modules by coupling the semiconductor with the thermal conduction, convection and radiation equations', *Energy Procedia*, vol. 77, pp. 215–224, Aug. 2015.

[42] J. Bisquert and I. Mora-Seró, 'Simulation of steady-state characteristics of dye-sensitized solar cells and the interpretation of the diffusion length', *J. Phys. Chem. Lett.*, vol. 1, no. 1, pp. 450–456, Jan. 2010.

[43] L. Andrade, J. Sousa, H. Aguilar Ribeiro, and A. Mendes, 'Phenomenological modeling of dye-sensitized solar cells under transient conditions', *Solar Energy*, vol. 85, no. 5, pp. 781–793, May 2011.

.